

# Discovery of Compton-thick quasars in the Sloan Digital Sky Survey

C. Vignali,<sup>1,2\*</sup> D. M. Alexander,<sup>3\*</sup> R. Gilli<sup>2\*</sup> and F. Pozzi<sup>1\*</sup>

<sup>1</sup> *Dipartimento di Astronomia, Università degli Studi di Bologna, Via Ranzani 1, 40127 Bologna, Italy*

<sup>2</sup> *INAF – Osservatorio Astronomico di Bologna, Via Ranzani 1, 40127 Bologna, Italy*

<sup>3</sup> *Department of Physics, Durham University, South Road, Durham DH1 3LE*

Accepted 2010 January 01. Received 2009 December 10; in original form 2009 June 26

## ABSTRACT

We present new and archival *Chandra* snapshot ( $\approx 10$  ks each) observations of 15 optically identified (from the Sloan Digital Sky Survey, SDSS) Type 2 quasars at  $z=0.40$ – $0.73$ . When combined with existing X-ray data, this work provides complete X-ray coverage for all 25 radio-quiet Type 2 quasars with  $\log L_{[\text{O III}]} > 9.28 L_{\odot}$  from Zakamska et al. (2003). Two targets out of 15 were not detected by *Chandra* and most of the remaining sources are X-ray weak, with nine having less than 10 counts in the 0.5–8 keV band. Low-to-moderate quality spectral analysis was limited to three sources, whose properties are consistent with the presence of column densities in the range  $N_{\text{H}} \approx 10^{22}$ – $10^{23}$  cm<sup>-2</sup> in the source rest frame. If the [O III] luminosity is a reliable proxy for the intrinsic X-ray luminosity, the current X-ray data indicate that Compton-thick quasars may hide among  $\approx 65$  per cent of the SDSS Type 2 quasar population ( $L_{\text{X,meas}}/L_{\text{X,[O III]}} < 0.01$ ); however, since the Type 2 quasar sample is selected on [O III] luminosity, the estimated Compton-thick quasar fraction may be overestimated. Using archival *Spitzer* observations, we find that  $\approx 50$  per cent of SDSS Type 2 quasars appear to be obscured by Compton-thick material based on both the  $L_{\text{X,meas}}/L_{\text{X,mid-IR}}$  (where mid-IR corresponds to rest-frame 12.3  $\mu\text{m}$ ) and  $L_{\text{X,meas}}/L_{\text{X,[O III]}}$  ratios. We use this information to provide an estimate of the Compton-thick quasar number density at  $z \approx 0.3$ – $0.8$ , which we find is in broad agreement with the expectations from X-ray background models.

**Key words:** quasars: general — galaxies: nuclei — galaxies: active

## 1 INTRODUCTION

Over the last decade, the quest for the identification of Type 2 quasars<sup>1</sup> has received renewed interest, and many sources or promising candidates of this class have been detected, mainly through X-ray surveys (e.g., Norman et al. 2002; Mainieri et al. 2002, 2007; Fiore et al. 2003; Gandhi et al. 2004, 2006; Mateos et al. 2005; Severgnini et al. 2006; Della Ceca et al. 2008; Krumpe et al. 2008). Predicted by unification schemes of AGN (e.g., Antonucci 1993), they are thought to play an important role in many synthesis models that seek to explain the origin of the X-ray background (XRB; e.g., Gilli, Comastri & Hasinger 2007). On the other hand, the availability of deep radio and *Spitzer* observations up to 24  $\mu\text{m}$  has allowed to define complementary methods to search for and characterize candidate Type 2 quasars (e.g.,

Martinez-Sansigre et al. 2005, 2008; Houck et al. 2005; Higdon et al. 2005, 2008; Weedman et al. 2006a,b,c; Dey et al. 2008; see also Donley et al. 2008 for a review), and examples of the most heavily obscured, Compton-thick AGN (with column density above  $\approx 10^{24}$  cm<sup>-2</sup>), have been possibly found (e.g., Alexander et al. 2005, 2008; Martinez-Sansigre et al. 2007; Daddi et al. 2007; Fiore et al. 2008, 2009, hereafter F09; Polletta et al. 2008; Lanzuisi et al. 2009).

An alternative approach to X-ray and mid-infrared (mid-IR) surveys for the quest of Type 2 quasars consists in following-up, in the X-ray band, promising Type 2 candidates selected through optical emission lines. In this regard, a careful selection on the basis of the [O III]5007  $\text{\AA}$  luminosity allowed Zakamska et al. (2003; hereafter Z03) to define a sample of 291 Sloan Digital Sky Survey (SDSS; York et al. 2000) Type 2 quasar candidates in the redshift range  $\approx 0.3$ – $0.8$  (see also Zakamska et al. 2004, 2005, 2006 and 2008, and Liu et al. 2009 for observations and properties of these objects at other wavelengths). These sources are classified on the basis of high-excitation, narrow emission lines, without underlying broad components, and with line ratios characteristic of non-stellar ionizing radiation. Standard AGN photo-ionization models are able to successfully reproduced most of the emission-line ratio

\* E-mail: cristian.vignali@unibo.it (CV); d.m.alexander@durham.ac.uk (DMA); roberto.gilli@oabo.inaf.it (RG); f.pozzi@unibo.it (FP).

<sup>1</sup> We defined Type 2 quasars as luminous ( $L_{2-10\text{keV}} > 10^{44}$  erg s<sup>-1</sup>) and obscured (column density  $N_{\text{H}} > 10^{22}$  cm<sup>-2</sup>) Active Galactic Nuclei - AGN - in X-rays, often characterized by high-ionization, narrow emission lines and the lack of broad emission lines in the rest-frame optical/ultraviolet spectra.

diagrams, at least for the most [O III]-luminous AGN in the Z03 sample (Villar-Martín et al. 2008).

In this context, the X-ray band is crucial to confirm the AGN nature of these sources and assess the presence of obscuration, given all the uncertainties related to obscured AGN selection on the basis of the [O III] emission line (see §4 for extended discussion). In Vignali, Alexander and Comastri (2004a, hereafter V04; see also Vignali, Alexander & Comastri 2004b), we presented the basic X-ray properties of a sub-sample of these Type 2 quasar candidates, mostly based on *ROSAT* observations. In Vignali, Alexander & Comastri 2006 (hereafter V06), we placed significant constraints on the fraction of heavily obscured, possibly Compton-thick AGN among the population of SDSS Type 2 AGN, being of the order of  $\approx 50$  per cent (see also Ptak et al. 2006 for similar findings from an X-ray perspective). We note that this result was possible by assuming the correlation between the [O III] and the 2–10 keV flux found for Seyfert 2 galaxies (Mulchaey et al. 1994; hereafter M94), which is characterized by a significant scatter. Unlike the Type 2 quasar population found in moderately deep and ultra-deep X-ray surveys, at the optical magnitude limit of the SDSS, Type 2 quasars are generally easy to study at both optical and X-ray wavelengths, as confirmed by the results obtained over the last four years through a snapshot strategy with both *Chandra* and *XMM-Newton*.

In this paper we extend the work shown by V04 and V06 by presenting *Chandra* observations for 12 additional SDSS Type 2 quasar candidates, thus providing a complete X-ray coverage for all 25 radio-quiet Type 2 quasars with  $\log L_{[\text{OIII}]} > 9.28 L_{\odot}$  from Z03. We have also included in our analyses three pointed *Chandra* observations retrieved from the public archive. Coupled with previous X-ray observations of AGN drawn from the original Z03 sample, the current targets bring the total number of sources with available *Chandra* and/or *XMM-Newton* constraints to 31 (74 per cent of X-ray detections, but see also Lamastra et al. 2009 for recent updates).

The work by Z03 has been recently expanded and updated by Reyes et al. (2008; hereafter R08), where the [O III]5007Å line luminosity is computed using both a Gaussian feature and a non-parametric line fitting method (see their Section 2.4). More than 90 per cent of the Type 2 quasar candidates reported by Z03 were recovered from this more complex analysis. Since our project was originally thought to provide a reliable and complete X-ray characterization of all the sources possibly classified as Type 2 quasars from the Z03 sample - a goal pursued by specific runs of observations with *Chandra* (see V06 and this paper) - we will keep the original [O III] line luminosities reported by Z03 and discuss how the differences with respect to R08 impact on our conclusions on the number density of Compton-thick quasars in §4.

The outline of the paper is as follows: in §2 the SDSS Type 2 quasar sample is presented, along with *Chandra* follow-up observations and X-ray spectral results, while §3 is focused on *Spitzer* observations and usage of the mid-IR luminosity as a proxy for the intrinsic X-ray luminosity, hence to pick up heavily obscured quasars. The space density of SDSS Compton-thick quasars is shown and extensively discussed in §4 in the light of current XRB model expectations and recent findings at higher redshifts. Finally, the main results are summarized in §5.

Hereafter we adopt the “concordance” (WMAP) cosmology ( $H_0=70 \text{ km s}^{-1} \text{ Mpc}^{-1}$ ,  $\Omega_M=0.3$ , and  $\Omega_{\Lambda}=0.7$ ; Spergel et al. 2003).

## 2 SAMPLE SELECTION AND CHANDRA OBSERVATIONS

The 12 sources of the main sample presented in this work were specifically selected for *Chandra* Cycle 8 observations on the basis of their luminous [O III] emission. Combined with previous sources targeted by *Chandra* (see V06 and Ptak et al. 2006), these observations provide a complete sampling of the luminous (i.e., in the quasar range) Type 2 AGN population revealed by the original study of Z03. In particular, using the M94 correlation between [O III] and hard X-ray flux, all the Z03 objects with predicted 2–10 keV luminosity above  $4 \times 10^{44} \text{ erg s}^{-1}$ , i.e., in the quasar regime, have been observed by *Chandra* and *XMM-Newton* (grey region in Fig. 1). The “membership” of all these sources to the “quasar locus” (above  $10^{44} \text{ erg s}^{-1}$ ) is valid even adopting the lowest X-ray luminosities predicted from the M94 correlation assuming its  $1\sigma$  uncertainty, i.e., the sources included in the grey region of Fig. 1 have predicted hard X-ray luminosities at least of  $10^{44} \text{ erg s}^{-1}$ . Only two sources in this “quasar locus” were not targeted, because they are radio loud (similarly to SDSS 081253.09+401859.9 of the archival sub-sample presented here), hence possibly not representative of the majority of the Type 2 quasar population, which is expected to be radio quiet. The main sample of 12 targets shown in Fig. 1 has been distinguished from the additional three sources retrieved from the *Chandra* archive on the basis of the size of the symbols (large and small open squares, respectively).

### 2.1 Chandra data reduction and analysis

The 12 SDSS Type 2 quasar candidates of the main sample were targeted by *Chandra* during Cycle 8 with the Advanced CCD Imaging Spectrometer (ACIS; Garmire et al. 2003) and the S3 CCD at the aimpoint; we used a snapshot strategy ( $\approx 10$  ks exposures) and very faint mode for the event telemetry format. The three archival observations, with similar exposures, were carried out during Cycle 7 in faint mode. Standard data reduction procedures were adopted using the *Chandra* Interactive Analysis of Observations (CIAO) Version 3.4 software. Source detection in the full (0.5–8 keV), soft (0.5–2 keV) and hard (2–8 keV) energy bands was carried out with WAVDETECT (Freeman et al. 2002) using a false-positive probability threshold of  $10^{-4}$ , which is less conservative than that typically adopted in source detection in X-ray survey fields, given the “a priori” knowledge of the source positions in our case. Limited intervals of high background were present in two observations and removed through the generation of new good-time intervals. The observation log is shown in Table 1; hereafter we will refer to the SDSS sources mostly using their abbreviated names.

In the total sample of 15 sources, only two targets were clearly not detected (SDSS J0149–0048 and SDSS J0921+5153), while all of the remaining sources were revealed by *Chandra*, although nine with less than 10 counts in the observed full band (see Table 2). These objects were carefully checked, following a procedure similar to that described in Vignali et al. (2001). Monte-Carlo simulations indicate that all of the sources with less than 10 counts, including the X-ray weak objects with 2–4 counts in the detection bands, are reliable detections (see last column of Table 2). From all these observations, coupled with those published by V06, we aim at deriving the basic X-ray properties (e.g., X-ray flux, hence luminosity, for all sources, and possibly photon index and absorption for the X-ray brightest targets) of SDSS Type 2 quasars.

**Table 1.** *Chandra* observation log for the SDSS Type 2 quasar candidates presented in this paper.

Src. ID #	Object Name SDSS J	$z$	X-ray ( $\alpha_{2000}$ )	X-ray ( $\delta_{2000}$ )	$\Delta_{\text{Opt-X}}$ (arcsec)	Obs. Date	Exp. Time (ks)
Sources observed as targets in Chandra AO8 – Main Sample							
9	005621.72+003235.8	0.484	00 56 21.7	+00 32 35.9	0.2	2008 Feb 08–09	9.91
16	012032.21–005502.0	0.601	01 20 32.2	–00 55 02.0	0.2	2007 Feb 18	9.83 <sup>a</sup>
20	013416.34+001413.6	0.555	01 34 16.3	+00 14 13.7	0.1	2007 Sep 10	9.91
29	014932.53–004803.7	0.566	.....	.....	.....	2007 Aug 30	10.01
30	015716.92–005304.8	0.422	01 57 16.9	–00 53 04.5	0.3	2007 Jun 18	9.92
100	073745.88+402146.5	0.613	07 37 45.9	+40 21 45.7	0.9	2007 Feb 03–04	9.33
153	092152.45+515348.1	0.587	.....	.....	.....	2007 Sep 27	10.04
182	102746.03+003205.0	0.614	10 27 46.0	+00 32 04.7	0.4	2007 Jan 13	9.91
186	103951.49+643004.2	0.402	10 39 51.5	+64 30 04.3	0.1	2007 Feb 04	9.52 <sup>a</sup>
205	122845.74+005018.7	0.575	12 28 45.7	+00 50 18.9	0.2	2007 Mar 12	9.42
232	144642.29+011303.0	0.725	14 46 43.0	+01 13 03.2	0.2	2007 Mar 22	10.04
244	151711.47+033100.2	0.613	15 17 11.5	+03 31 00.3	0.1	2007 Mar 28	9.91
Archival Sample							
18	012341.47+004435.9	0.399	01 23 41.5	+00 44 35.9	0.2	2006 Feb 07–08	9.83
117	081253.09+401859.9	0.551	08 12 53.1	+40 19 00.5	0.6	2005 Dec 11	9.89
152	092014.11+453157.3	0.402	09 20 14.1	+45 31 56.9	0.4	2006 Mar 05	10.05

The source ID is taken from Table 1 of Z03. The optical positions of the quasars can be drawn from their SDSS name, while the X-ray positions for the X-ray detected sources have been obtained from either WAVDETECT or the centroid of the source count distribution using the full-band image. We note that also the sources from the archival sample were targets of pointed *Chandra* observations (Cycle 7). <sup>a</sup> Corrected for high-background periods.

## 2.2 X-ray spectral analysis

Among the 15 targets analyzed in this paper, low-to-moderate quality X-ray spectral analysis was possible only for three sources, having a number of full-band counts in the range  $\approx 50$ –200: SDSS J1228+0050 (main sample), SDSS J0123+0044 and SDSS J0812+4018 (archival sample; see Table 2).

Spectral analysis was carried out with XSPEC Version 11.3.2 (Arnaud 1996) using unbinned data and the  $C$ -statistic (Cash 1979; Nousek and Shue 1989) for source SDSS J1228+0050, while for the other two sources data were binned to at least 10 counts per bin. Errors are quoted at the 90 per cent confidence level for one interesting parameter ( $\Delta C = 2.71$ ; Avni 1976; Cash 1979), unless stated otherwise. Galactic absorption (from Dickey and Lockman 1990; see Table 3) was included in all the spectral fittings.

The limited energy band allowed by *Chandra*, coupled to the poor counting statistics, prevents us from an accurate estimate of the source spectral parameters. Having said that, we note that a fitting with a power-law model provides a flat photon index for all of the sources ( $\Gamma = -0.31_{-0.43}^{+0.40}$ ,  $\Gamma = -0.16_{-0.37}^{+0.36}$  and  $\Gamma = 1.22 \pm 0.22$  for SDSS J1228+0050, SDSS J0123+0044 and SDSS J0812+4018, respectively). In the light of the optical classification of these sources, the interpretation of the flatness of the X-ray spectrum (if compared to that typically expected from Type 1 quasars; see, e.g., Piconcelli et al. 2005 and references therein) as due to absorption at the source provides a reliable representation of the X-ray data. Indeed, the inclusion of absorption provides a more reliable fitting in term of resulting photon indices, which become consistent with those typically observed in Type 1 AGN (Page et al. 2005).<sup>2</sup> The derived column densities are  $1.52_{-0.83}^{+1.30} \times 10^{23} \text{ cm}^{-2}$  (SDSS J1228+0050),  $1.44_{-0.37}^{+0.49} \times 10^{23} \text{ cm}^{-2}$  (SDSS J0123+0044)

and  $2.14_{-0.81}^{+1.15} \times 10^{22} \text{ cm}^{-2}$  (SDSS J0812+4018; see Table 3). We note that the source with the lowest measured X-ray absorption is SDSS J0812+4018, which is also radio loud, with a radio loudness parameter<sup>3</sup> of  $\approx 4300$ . The interpretation of the X-ray data for this source is complicated by its radio-loud nature; we note that in this case absorption could be ascribed to gas entrained by the unresolved radio jet (which may be responsible also for part of the X-ray emission), although no firm conclusions can be drawn from the current X-ray data.

For what concerns the remaining X-ray detected sources, we were able to provide some constraints on the absorption only for SDSS J0157–0053; its hardness ratio [defined as  $\text{HR}=(\text{H}-\text{S})/(\text{H}+\text{S})$ , where H and S are the source counts in the hard and soft bands, respectively] of  $0.48 \pm 0.32$  is suggestive of a column density of  $\approx 5 \times 10^{22} - 10^{23} \text{ cm}^{-2}$ .

## 2.3 X-ray results: discussion

In this paper, as well as in V06, we have shown that the population of SDSS Type 2 quasar candidates investigated by *Chandra* is characterized by low X-ray emission, in comparison with that expected from the [O III]5007Å emission-line intensity and the M94 correlation. In the following discussion, we consider all of the sources with either a *Chandra* or XMM-Newton observation. We note that for six sources for which we refer to *Chandra* data, XMM-Newton observations are also present in the archive; in particular, four of these six objects were observed as targets by XMM-Newton. Of these six sources, we have only one detection; for the other sources, the

<sup>2</sup>  $\Gamma = 2.6_{-0.6}^{+0.5}$  for SDSS J0812+4018, while was fixed to  $\Gamma = 2.0$  for source SDSS J0123+0044.

<sup>3</sup> Radio-loudness parameter, defined as  $R = f_{5 \text{ GHz}}/f_{4400 \text{ Å}}$  (where 5 GHz and 4400 Å are both rest frame; Kellermann et al. 1989).

<sup>2</sup> The resulting photon index is  $\Gamma = 1.9_{-1.2}^{+1.6}$  for SDSS J1228+0050 and

**Table 2.** X-ray counts, count rates, and results from Monte-Carlo simulations.

Source Name	X-ray net counts			Count rate	Det. Sign. <sup>a</sup>	
	SDSS J	[0.5–2 keV]	[2–8 keV]	[0.5–8 keV]		
0056+0032		2.9 <sup>+2.9</sup> <sub>-1.6</sub>	< 3.0	2.9 <sup>+2.9</sup> <sub>-1.6</sub>	2.93 [1.31–5.85] × 10 <sup>-4</sup>	3.6 ... 2.9
0120–0055		1.9 <sup>+2.6</sup> <sub>-1.3</sub>	1.8 <sup>+2.6</sup> <sub>-1.2</sub>	3.7 <sup>+3.1</sup> <sub>-1.8</sub>	3.77 [1.93–6.92] × 10 <sup>-4</sup>	4.0 3.3 4.8
0134+0014		1.8 <sup>+2.6</sup> <sub>-1.2</sub>	< 4.8	2.7 <sup>+2.9</sup> <sub>-1.5</sub>	2.73 [1.21–5.85] × 10 <sup>-4</sup>	3.6 ... 4.0
0149–0048		< 4.8	< 3.0	< 4.8	< 4.80 × 10 <sup>-4</sup>	
0157–0053		5.9 <sup>+3.6</sup> <sub>-2.4</sub>	16.7 <sup>+5.2</sup> <sub>-4.0</sub>	22.7 <sup>+5.8</sup> <sub>-4.7</sub>	2.29 [1.82–2.87] × 10 <sup>-3</sup>	
0737+4021		1.9 <sup>+2.6</sup> <sub>-1.3</sub>	2.8 <sup>+2.9</sup> <sub>-1.6</sub>	4.7 <sup>+3.3</sup> <sub>-2.1</sub>	5.03 [3.00–8.58] × 10 <sup>-4</sup>	3.7 4.1 5.5
0921+5153		< 4.8	< 3.0	< 4.8	< 4.78 × 10 <sup>-4</sup>	
1027+0032		2.9 <sup>+2.9</sup> <sub>-1.6</sub>	< 3.0	2.7 <sup>+2.9</sup> <sub>-1.5</sub>	2.72 [1.21–5.85] × 10 <sup>-4</sup>	4.7 ... 3.3
1039+6430		4.0 <sup>+3.2</sup> <sub>-1.9</sub>	< 6.4	5.9 <sup>+3.6</sup> <sub>-2.4</sub>	6.20 [3.68–9.98] × 10 <sup>-4</sup>	5.7 ... 5.7
1228+0050		6.0 <sup>+3.2</sup> <sub>-1.9</sub>	44.4 <sup>+7.7</sup> <sub>-6.6</sub>	50.4 <sup>+8.2</sup> <sub>-7.1</sub>	5.35 [4.60–6.22] × 10 <sup>-3</sup>	
1446+0113		5.9 <sup>+3.6</sup> <sub>-2.4</sub>	< 3.0	5.8 <sup>+3.6</sup> <sub>-2.3</sub>	5.78 [3.49–9.37] × 10 <sup>-4</sup>	6.4 ... 5.5
1517+0331		2.9 <sup>+2.9</sup> <sub>-1.6</sub>	< 3.0	2.7 <sup>+2.9</sup> <sub>-1.5</sub>	2.72 [1.21–5.65] × 10 <sup>-4</sup>	4.4 ... 3.8
0123+0044		13.5 <sup>+4.8</sup> <sub>-3.6</sub>	145.2 <sup>+13.1</sup> <sub>-12.0</sub>	161.2 <sup>+13.7</sup> <sub>-12.7</sub>	1.64 [1.51–1.78] × 10 <sup>-2</sup>	
0812+4018		128.6 <sup>+12.4</sup> <sub>-11.3</sub>	72.0 <sup>+9.5</sup> <sub>-8.5</sub>	199.8 <sup>+15.2</sup> <sub>-14.1</sub>	2.02 [1.88–2.17] × 10 <sup>-2</sup>	
0920+4531		6.8 <sup>+3.8</sup> <sub>-2.5</sub>	< 6.4	9.4 <sup>+4.2</sup> <sub>-3.0</sub>	9.36 [6.37–13.54] × 10 <sup>-4</sup>	7.2 ... 7.9

The source names are abbreviated on the basis of the four RA and DEC digits. Errors on the X-ray net counts (i.e., background-subtracted) were computed according to Gehrels (1986). The upper limits are at the 95% confidence level and were computed according to Kraft, Burrows & Nousek (1991). <sup>a</sup> Significance of the detection (in units of  $\sigma$ ) in the soft band, hard band, and full band, respectively, estimated using the Monte-Carlo method described in Vignali et al. (2001) and applied only to sources with less than 10 counts.

**Table 3.** Properties of the SDSS Type 2 quasars observed by *Chandra*.

Object	$N_{\text{Hgal}}$	$\log L_{[\text{OIII}]}$	$F_{2-10 \text{ keV}}$	$N_{\text{H}_z}$	$L_{2-10 \text{ keV}}$	$L_{2-10 \text{ keV}}$ (pr.)	$S_{1.4 \text{ GHz}}$	
(1)	(2)	(3)	(4)	(5)	(6)	(7)	(8)	(9)
0056+0032	2.79	9.45	1.0 × 10 <sup>-15</sup>		8.9 × 10 <sup>41</sup>	1.5 × 10 <sup>44</sup> –2.6 × 10 <sup>45</sup>	8.60	8.33
0120–0055	3.69	9.28	1.4 × 10 <sup>-15</sup>		2.1 × 10 <sup>42</sup>	1.0 × 10 <sup>44</sup> –1.8 × 10 <sup>45</sup>	< 0.144	
0134+0014	2.48	9.53	9.6 × 10 <sup>-16</sup>		1.2 × 10 <sup>42</sup>	1.8 × 10 <sup>44</sup> –3.2 × 10 <sup>45</sup>	< 0.201	
0149–0048	2.55	9.36	< 1.7 × 10 <sup>-15</sup>		< 2.2 × 10 <sup>42</sup>	1.2 × 10 <sup>44</sup> –2.1 × 10 <sup>45</sup>	1.03	1.60
0157–0053	2.58	9.52	8.1 × 10 <sup>-15</sup>		5.2 × 10 <sup>42</sup>	1.8 × 10 <sup>44</sup> –3.1 × 10 <sup>45</sup>	< 0.135	
0737+4021	6.18	9.28	1.9 × 10 <sup>-15</sup>		3.0 × 10 <sup>42</sup>	1.0 × 10 <sup>44</sup> –1.8 × 10 <sup>45</sup>	< 0.134	
0921+5153	1.27	9.28	< 1.6 × 10 <sup>-15</sup>		< 2.3 × 10 <sup>42</sup>	1.0 × 10 <sup>44</sup> –1.8 × 10 <sup>45</sup>	2.37	2.49
1027+0032	4.47	9.36	1.0 × 10 <sup>-15</sup>		1.6 × 10 <sup>42</sup>	1.2 × 10 <sup>44</sup> –2.1 × 10 <sup>45</sup>	3.25	3.09
1039+6430	1.18	9.41	2.1 × 10 <sup>-15</sup>		1.2 × 10 <sup>42</sup>	1.4 × 10 <sup>44</sup> –2.4 × 10 <sup>45</sup>	< 0.5	
1228+0050	1.88	9.28	1.8 × 10 <sup>-14</sup>	1.52 <sup>+1.30</sup> <sub>-0.83</sub> × 10 <sup>23</sup>	3.5 × 10 <sup>43</sup>	1.0 × 10 <sup>44</sup> –1.8 × 10 <sup>45</sup>	3.14	2.95
1446+0113	3.55	9.37	2.1 × 10 <sup>-15</sup>		5.0 × 10 <sup>42</sup>	1.3 × 10 <sup>44</sup> –2.2 × 10 <sup>45</sup>	5.75	5.75
1517+0331	3.78	9.36	9.8 × 10 <sup>-16</sup>		1.5 × 10 <sup>42</sup>	1.2 × 10 <sup>44</sup> –2.1 × 10 <sup>45</sup>	< 0.150	
0123+0044	3.24	9.13	5.8 × 10 <sup>-14</sup>	1.44 <sup>+0.49</sup> <sub>-0.37</sub> × 10 <sup>23</sup>	3.4 × 10 <sup>44</sup>	7.3 × 10 <sup>43</sup> –1.3 × 10 <sup>45</sup>	11.83	11.34
0812+4018	5.16	9.39	7.5 × 10 <sup>-14</sup>	2.14 <sup>+1.15</sup> <sub>-0.81</sub> × 10 <sup>22</sup>	1.7 × 10 <sup>44</sup>	1.3 × 10 <sup>44</sup> –2.3 × 10 <sup>45</sup>	1067.88	1058.83
0920+4531	1.51	9.04	3.2 × 10 <sup>-15</sup>		1.8 × 10 <sup>42</sup>	5.9 × 10 <sup>43</sup> –1.0 × 10 <sup>45</sup>	< 0.5	

(1) Abbreviated SDSS name; (2) Galactic column density, from Dickey & Lockman (1990), in units of 10<sup>20</sup> cm<sup>-2</sup>; (3) log of the [OIII] line luminosity, in units of  $L_{\odot}$  (from Z03); (4) Galactic absorption-corrected flux (or upper limit, in units of erg cm<sup>-2</sup> s<sup>-1</sup>) in the 2–10 keV band, extrapolated from the observed 0.5–8 keV count rate or upper limit assuming a power law with  $\Gamma = 2.0$  (typical for AGN X-ray emission). We note that assuming a pure cold reflection spectrum, parameterized here as a power-law with  $\Gamma = 0$ , would increase the *observed* 2–10 keV flux by a factor of  $\approx 8$ ; (5) intrinsic column density, obtained from the best-fit X-ray spectral fitting, when possible, in units of cm<sup>-2</sup>; (6) 2–10 keV rest-frame luminosity, obtained through the observed flux (or upper limit), corrected for the effect of intrinsic absorption (when the column density can be measured directly from the spectral fit), in units of erg s<sup>-1</sup>; in case of a reflection spectrum, the *rest-frame* 2–10 keV luminosity would increase by a factor of  $\approx 3$ . (7) 2–10 keV luminosity range predicted from the [O III] line vs. hard X-ray flux correlation (M94), in units of erg s<sup>-1</sup>; the interval is given by the  $\pm 1\sigma$  values around the mean M94 correlation; (8)–(9) integrated (8) and peak (9) radio flux density (or  $1\sigma$  upper limits) at 1.4 GHz, all from the FIRST (Becker, White & Helfand 1995) except for SDSS J1039+6430, whose upper limit comes from the NVSS (Condon et al. 1998), in units of mJy. We note that for SDSS J1027+0032 the optical–radio association is dubious, since the distance between the radio and optical position is large (1.0'').

All luminosities are computed using  $H_0 = 70$  km s<sup>-1</sup> Mpc<sup>-1</sup>,  $\Omega_M = 0.3$ , and  $\Omega_{\Lambda} = 0.7$ .

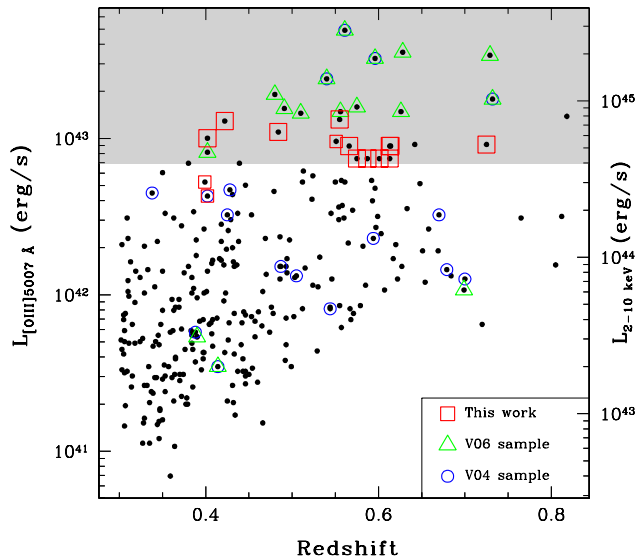


**Figure 1.** Logarithm of the measured  $L_{[\text{O III}]}$  luminosity (not corrected for extinction within the narrow-line region) vs. redshift for all of the sources in the Zakamska et al. (2003) catalog (small filled circles). At the right of the panel, the 2–10 keV luminosity, estimated using the  $[\text{O III}]$  emission and the M94 correlation, are shown. The key provides a description of the X-ray observations; in particular, the sources presented in this paper are plotted as open squares (the three small open squares refer to the objects whose observations were retrieved from the *Chandra* archive). The grey region defines the locus of the AGN with  $\log L_X > 44.6 \text{ erg s}^{-1}$ , where the AGN still lie in the quasar luminosity range ( $\log L_X > 44 \text{ erg s}^{-1}$ ) even assuming the  $1\sigma$  error around the mean of the original correlation between  $[\text{O III}]$  and hard X-rays. We note that all of the objects in the grey region have been observed in X-rays except for two sources which are radio loud.

integration time is typically lower or comparable to that of *Chandra* observations, once the intervals of high particle background (flares) are removed. This means that the constraints achieved using *Chandra* data for these six sources remain the best available to date. About the source detected by *XMM-Newton*, it was already detected by *Chandra* (src. #15; V06) and was bright enough for an X-ray spectral extraction. However, we note that the presence of diffuse X-ray emission in the *XMM-Newton* observation within the aperture adopted for X-ray spectral extraction may provide some contamination to the AGN properties, as shown by the source flux which is  $\approx 70$  per cent higher than in the *Chandra* observation. For this reason, we prefer to use the *Chandra* constraints (as reported in V06) also for this source.

If we correct the X-ray luminosity accounting for the measured absorption (when a column density estimate is feasible through spectral analysis, see the filled squares and triangles in Fig. 2; the measured column densities are in the range  $\approx 1.5 \times 10^{22} - 4.3 \times 10^{23} \text{ cm}^{-2}$ , see V06 and §2.2), we generally find a good agreement between the expected and the observed 2–10 keV luminosity. On the other hand, there is a significant fraction of Type 2 AGN candidates ( $\approx 65$  per cent) whose observed luminosity is less than 1 per cent of the predicted one; for these sources, heavy obscuration towards the nuclear source appears a reasonable explanation for their weak X-ray emission, supported by the optical classification of Z03 (see also Ptak et al. 2006 for similar conclusions, and the recent results of LaMassa et al. 2009 using a

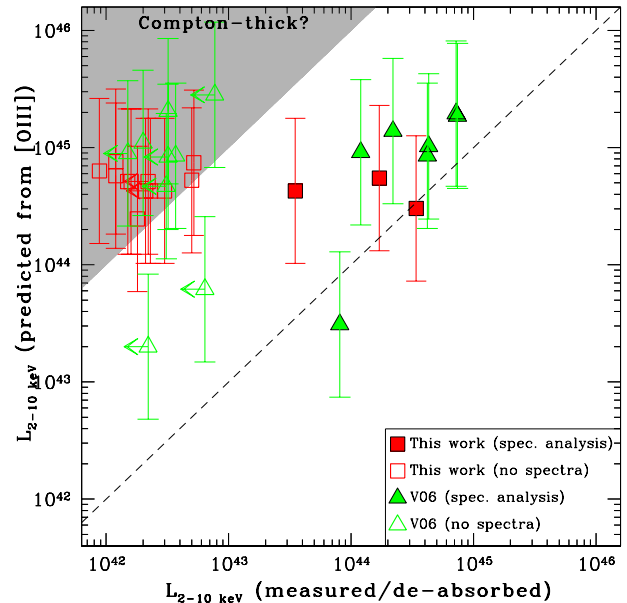


**Figure 2.** Comparison of the 2–10 keV rest-frame luminosity computed from the available X-ray data with that predicted assuming the M94 correlation (i.e., derived from the  $[\text{O III}]$  luminosity). The dashed line shows the 1:1 ratio between the two X-ray luminosities. All of the sources with either a *Chandra* or *XMM-Newton* observation are shown. For the filled symbols (squares: data presented in this paper; triangles: data in V06), the X-ray luminosity is de-absorbed on the basis of the column density derived from the best-fitting model (see Table 3); for all of the remaining sources, the X-ray luminosity is derived from the X-ray flux with no correction for the unknown column density. Sources with X-ray spectral results at the center of the plot are obscured, with typical measured column densities of a few  $\times 10^{22} - 5 \times 10^{23} \text{ cm}^{-2}$ , while the upper-left grey region shows the locus of extremely obscured, likely Compton-thick sources, where the observed luminosity is  $\lesssim 1$  per cent of the predicted one. Leftward arrows indicate upper limits on the observed X-ray luminosity.

lower redshift sample of SDSS Seyfert 2 galaxies). Hereafter, we will assume the sources with measured/predicted X-ray luminosity less than 0.01 as probably Compton thick. This is a conservative threshold since there are known Compton-thick AGN in the local Universe with more than 1 per cent of observed over intrinsic X-ray emission (e.g., NGC 6240 and the Circinus galaxy; Bassani et al. 1999; Matt et al. 2000; see also Maiolino et al. 1998, where this fraction is  $\approx 2$  per cent for a sample of Compton-thick Seyfert 2 galaxies).

Similarly to V06, we did not correct the  $[\text{O III}]$  flux to account for the absorption due the narrow-line region (NLR) itself (for details, see Maiolino et al. 1998; Bassani et al. 1999; Panessa et al. 2006, hereafter P06; see also Lamastra et al. 2009), because the SDSS spectral coverage does not typically cover the rest-frame wavelengths necessary to measure the emission-line fluxes of  $\text{H}\beta$  and  $\text{H}\alpha$ , hence to use the  $\text{H}\alpha/\text{H}\beta$  ratio as extinction measurement. Using the ratio of higher order Balmer lines (e.g.,  $\text{H}\beta/\text{H}\gamma$ ,  $\text{H}\gamma/\text{H}\delta$ ) to estimate extinction represents a difficult task, due to their weakness over often noisy spectra. This approach implies that the predicted X-ray luminosities would be even higher for at least some sources, thus generally requiring a larger column density to account for the observed luminosities.

Furthermore, we have assumed the correlation between the  $[\text{O III}]$  emission-line intensity and the hard X-ray emission from

M94, which is based on a large sample ( $> 100$ ) of local Seyfert galaxies. As reported in Table 3, our objects have X-ray luminosities well below those predicted by the M94 correlation; 13 out of the 15 targets have X-ray measured/predicted luminosity ratios ( $L_{X,\text{meas}}/L_{X,[\text{O III}]}$ ) in the range  $\approx 0.001 - 0.081$  (where for the predicted X-ray luminosity, the “central” value from the M94 correlation has been assumed).

A few caveats must be considered before comparing different [O III] vs. hard X-ray correlations. If a pure cold reflection spectrum, roughly parameterized here as a flat ( $\Gamma = 0$ ) power-law slope, were present in the observed 0.5–8 keV band covered by *Chandra*, the 2–10 keV fluxes reported in Table 3 would increase by a factor  $\approx 8$ , and the rest-frame 2–10 keV luminosities by a factor  $\approx 3$ . Still a significant ( $\approx 40$ –50 per cent) fraction of SDSS Type 2 quasars would populate the Compton-thick locus in Fig. 2. We note, however, that studies of local reflection-dominated AGN indicate that a scattering component is possibly present in such cases (e.g., Comastri 2004), mostly “contaminating” the soft X-ray band; this would produce softer spectra and, as a consequence, any column density estimated through low-to-moderate quality X-ray spectral information would be under-estimated.

Since M94 work, many authors have searched for the presence of a correlation between the [O III] emission-line intensity and the hard X-rays. H05 clearly show the differences in deriving such correlation from an optically selected sample. In particular, they found that  $\log(L_{2-10\text{keV}}/L_{[\text{O III}]})$  is 1.59 (dispersion  $\sigma=0.48$ ) for optically ([O III]) selected Type 1 AGN, while  $\log(L_{2-10\text{keV}}/L_{[\text{O III}]})=0.57$  (dispersion  $\sigma=1.06$ ) for optically selected Type 2 AGN. We remind that the best-fit ratio assumed throughout this paper is  $L_{2-10\text{keV}}/L_{[\text{O III}]} \approx 1.8$  ( $\sigma \approx 0.6$ ), similar for Type 1 and Type 2 AGN (M94); this value is not significantly different from that of Type 1 AGN in H05. Under the basic assumption (unified schemes) that the intrinsic  $L_{2-10\text{keV}}/L_{[\text{O III}]}$  should be the same for Type 1 and Type 2 AGN, the only difference being the obscuration/extinction of the nuclear emission, to report our predicted X-ray luminosities (reported in Table 3 and shown in Fig. 2) into those of H05 we have to divide them by  $\approx 1.5$ . Given the significant dispersion of H05 correlation, a large fraction of sources ( $\approx 50$  per cent) would still be in the locus of heavily obscured, possibly Compton-thick quasars.

Finally, we note that the correlation found by P06 produces even larger hard X-ray luminosities than those reported in this paper (see also §4). For consistency with the assumptions of V04 and V06 which, combined with the present work, provide a complete X-ray coverage of all radio-quiet Type 2 quasars with  $\log L_{[\text{O III}]} > 9.28 L_{\odot}$  selected from Z03, we have decided to adopt the M94 correlation, keeping in mind all the caveats concerning both the selection criteria of the different samples and the significant dispersion in all of the correlations presented above; for further discussion, refer to §4. Support to the reliability of the [O III]-X-ray correlation is also provided by *Spitzer* data (see §3).

### 3 NEAR AND MID-IR OBSERVATIONS OF SDSS TYPE 2 QUASARS

#### 3.1 *Spitzer* data reduction and analysis

In the following, we estimate the nuclear power of the AGN by means of the rest-frame 5.8 $\mu\text{m}$  and 12.3 $\mu\text{m}$  luminosities, providing a robust support to the results from X-ray analysis. To this purpose, we retrieved from the *Spitzer* archive both IRAC and MIPS photometric observations for 20 SDSS Type 2 quasars in common with

those reported in this work and in V04a and V06. Most of these sources were targeted by *Spitzer* to get insights, for the first time, on the near-IR and mid-IR properties of a well defined sample of optically selected Type 2 AGN.

In particular, by these infrared data, we intend to provide an adequate complement to the X-ray investigation presented in the previous sections. The X-ray properties of these sources have been published mostly in V06 and Ptak et al. (2006); for seven of these sources, X-ray data are presented here. While IRAC covers the near-infrared (near-IR) and mid-IR bands with four channels (3.6, 4.5, 5.8 and 8 $\mu\text{m}$ ), MIPS allows for investigations at longer wavelengths (24, 70 and 160 $\mu\text{m}$ ), although in this work only 24 $\mu\text{m}$  data have been used.

For both IRAC and MIPS, we used the final post-calibrated data (PBCD) produced by the *Spitzer* Science Center (SSC) pipeline (Version 14.0.0 and 16.1.0, respectively). The flux densities in the IRAC and MIPS bands were measured on the signal maps using aperture photometry. The chosen aperture radius for the IRAC bands was 2.45", and the adopted factors for the aperture corrections are 1.21, 1.23, 1.38 and 1.58 (following the IRAC Data Handbook) at 3.6 $\mu\text{m}$ , 4.5 $\mu\text{m}$ , 5.8 $\mu\text{m}$ , and 8 $\mu\text{m}$ , respectively. The aperture radius for the 24 $\mu\text{m}$  MIPS band was 7", and the resulting aperture flux density was corrected adopting a factor of 1.61 (see the MIPS Data Handbook).

All of the quasars have been detected by *Spitzer*, spanning a flux density range at 8 $\mu\text{m}$  (24 $\mu\text{m}$ ) of  $\approx 0.11$  mJy ( $\approx 1.46$  mJy; source ID=290, the faintest object in the current sample) to  $\approx 12.8$  mJy ( $\approx 56.4$  mJy; source ID=197, the brightest source). Only four sources show indications of limited contamination by a nearby companion; however, in all of these cases the nearby source shows a decreasing flux density at longer wavelengths, suggesting a stellar or galaxy origin for its near-IR/mid-IR emission. The rest-frame 5.8 $\mu\text{m}$  and 12.3 $\mu\text{m}$  luminosities (Table 4) were derived via simple interpolation between nearby bands in the source rest frame; this method avoids that the results are dependent upon the assumption of particular AGN (torus) templates to reproduce the observed data points. Furthermore, we checked our results against the 14.5 $\mu\text{m}$  luminosities obtained using IRS spectra and reported by Zakamska et al. (2008) for eight sources in common, and found a relatively good agreement. The combined statistical and systematic errors associated to these mid-IR luminosities are  $\approx 10$ –15 per cent. In Table 4, also basic X-ray information and corresponding reference paper are presented.

#### 3.2 Mid-IR luminosity as a proxy of the X-ray emission

The rest-frame 5.8 $\mu\text{m}$  and 12.3 $\mu\text{m}$  luminosities (reported in Table 4) have been used to estimate the intrinsic, rest-frame 2–10 keV luminosities ( $L_{X,\text{mid-IR}}$ ) assuming the relations provided by F09 and Gandhi et al. (2009; hereafter G09), respectively.

The former relation,<sup>4</sup> parameterized by  $\log L_{2-10\text{keV}} = 43.57 + 0.72 \times (\log 158 - 44.2)$ , has been calibrated using Type 1 AGN in the *Chandra* Deep Field-South (CDF-S; Brusa et al. 2010) and in the *Chandra* Cosmic Evolution Survey (C-COSMOS; Civano et al., in preparation); for further details, see §3.3 and Fig. 5 in F09. This relation is similar (both in slope and intercept) to that recently derived by Lanzuisi et al. (2009) from a sample of

<sup>4</sup> This relation is valid if the criterion  $\log 158 > 43.04$  is satisfied, as in the case of all of our sources; see F09 for details.

**Table 4.** Properties of the SDSS Type 2 quasars observed by *Spitzer* IRAC and MIPS.

ID	Src. Name	$z$	$\log l58$ ( $L_{\odot}$ )	$\log (\lambda L_{\lambda})_{12.3\mu\text{m}}$ ( $L_{\odot}$ )	X-ray info	$\log L_X$
(1)	(2)	(3)	(4)	(5)	(6)	(7)
9	005621.72+003235.8	0.484	11.3	11.6	D/C/V09	41.95
18	012341.47+004435.9	0.399	11.2	11.2	D+/C/V09	44.53
20	013416.34+001413.6	0.555	11.2	11.5	D/C/V09	42.08
30	015716.92-005304.8	0.422	10.7	10.9	D/C/V09	42.72
34	021047.01-100152.9	0.540	11.2	11.3	D/X/V06	44.34
83	031950.54-005850.6	0.626	11.0	11.2	D/C/V06	42.57
113	080154.24+441234.0	0.556	11.2	11.4	D+/C/V06	44.62
117	081253.09+401859.9	0.551	11.4	11.4	D+/C/V09	44.23
119	081507.42+430427.2	0.510	11.8	11.8	ND/C/V06	< 42.51
130	084234.94+362503.1	0.561	10.9	11.4	ND/C/V06	< 42.89
152	092014.11+453157.3	0.402	11.3	11.5	D/C/V09	42.26
186	103951.49+643004.2	0.402	11.6	11.7	D/C/V09	42.08
196	115314.36+032658.6	0.575	11.2	11.3	D+/C/V06	44.08
197	115718.35+600345.6	0.491	12.1	12.2	ND/C/V06	< 42.18
204	122656.48+013124.3	0.732	11.6	11.6	D+/X/V06	44.63
207	123215.81+020610.0	0.480	11.1	11.3	D/C/V06	42.30
239	150117.96+545518.3	0.338	10.7	10.9	D/R/V04	44.24
256	164131.73+385840.9	0.596	11.6	11.8	D+/X/V06	44.87
289	235818.87-000919.5	0.402	10.6	10.9	ND/C/V06	< 42.49
290	235831.16-002226.5	0.628	10.3	10.8	D/C/V06	42.51

(1) Source ID (from Table 1 of Z03); (2) SDSS source name; (3) source redshift; (4) log of the luminosity at 5.8  $\mu\text{m}$  (rest frame), in units of  $L_{\odot}$ ; (5) log of the luminosity at 12.3  $\mu\text{m}$  (rest frame), in units of  $L_{\odot}$ ; (6) available X-ray information: the first term indicates whether the source has been detected in X-rays (D: detected; D+: detected and X-ray spectrum available; ND: undetected); the second term indicates the X-ray satellite whose data have been used to obtain information (C: *Chandra*; X: *XMM-Newton*; R: *ROSAT/RASS*). The last term indicates the reference paper (where V09 means the current work); (7) logarithm of the rest-frame 2–10 keV luminosity ( $\text{erg s}^{-1}$ ) or upper limit when the source is undetected. When an X-ray spectrum is available, the X-ray luminosity has been corrected to account for the measured absorption.

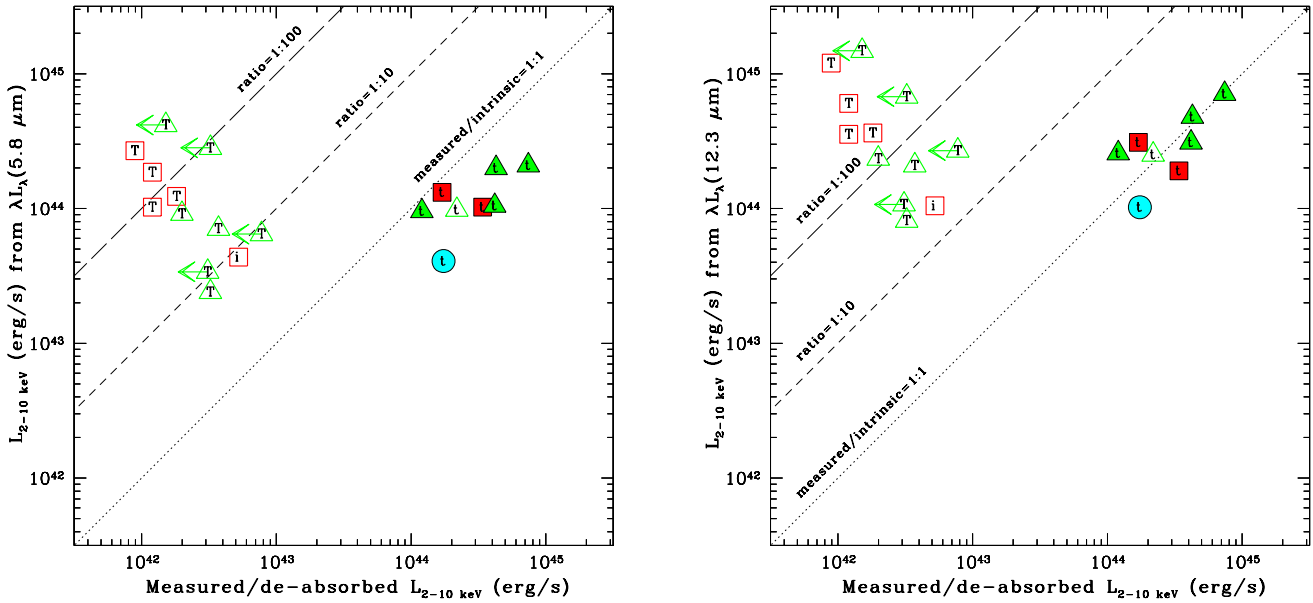


**Figure 3.** Comparison of the 2–10 keV luminosity computed from the available X-ray data with that predicted from the mid-IR luminosity at 5.8  $\mu\text{m}$  (rest frame) assuming the Fiore et al. (2009) correlation (*left panel*) and at 12.3  $\mu\text{m}$  (rest frame), using the Gandhi et al. (2009) correlation (*right panel*). The dotted, short-dashed and long-dashed lines indicate ratios of 1:1, 1:10 and 1:100 between the measured and the predicted X-ray luminosity. Symbols are the same as in Fig. 2; the filled circle marks the source with *ROSAT* (RASS) detection (V04). The letter inside each symbol indicates whether the source is a Compton-thick (T) or a Compton-thin (t) AGN candidate on the basis of the [O III]-driven results presented in §2.3 and shown in Fig. 2; for one object, the analysis does not lean towards any of the two classifications [hence we have an “intermediate” (i) AGN], although HR analysis suggests Compton-thin absorption.

SWIRE sources with X-ray coverage. For comparison, the assumption of the Lutz et al. (2004) relation between the  $6\mu\text{m}$  and hard X-ray luminosity derived using a sample of 71 local, moderate-luminosity Seyfert galaxies with low-resolution *ISO* spectra would predict larger X-ray luminosities given the mid-IR luminosities of our sample (see below for details).

The latter relation, parameterized by  $\log L_{2-10\text{ keV}} = (\log(\lambda L_\lambda)_{12.3\mu\text{m}} + 4.37)/1.11$ , has been obtained from a sample of 42 Seyfert galaxies with near diffraction-limited mid-IR imaging obtained with the VISIR instrument at the *VLT* (G09; see also Horst et al. 2006, 2008 and 2009).

All of these correlations are based on the assumption that the mid-IR band provides a clear view of the AGN nuclear activity, which is more affected by extinction and absorption at optical, ultraviolet and X-ray frequencies. However, a few issues must be taken into account in the following discussion. X-ray information is typically obtained from all the available data in literature work or in archives (from *ASCA* to *BeppoSAX*, up to the current X-ray missions); we note, however, that F09 and Lanzuisi et al. (2009) use only data with moderate (a few arcsec; *XMM-Newton*) to high (below  $1''$ ; *Chandra*) resolution, providing overall a relatively good match with *Spitzer* imaging data in terms of angular resolution.<sup>5</sup> On the one hand, G09 mid-IR data are characterized by sub-arcsec resolution (corresponding to physical scales of less than half parsec) matched to a broad variety of X-ray data, including old (*ASCA*) and recent (*Suzaku*) observations. While host galaxy contribution to hard X-ray emission, at the AGN luminosities probed by most of their sources (above  $10^{42}\text{ erg s}^{-1}$ ), is likely negligible (although some reprocessed emission may be present), it can still contaminate the mid-IR data at some level. On the other hand, at the median redshift ( $z \approx 1.5$ ) of the Type 1 AGN used by F09, the mid-IR emission would probe physical scales of  $\approx 20\text{ kpc}$ . Finally, Lutz et al. (2004) *ISO* spectra are characterized by  $24'' \times 24''$  apertures (corresponding to physical scales of a few kpc), including, in many cases, noticeable host galaxy emission, as pointed out by the authors.

The results are shown in Fig. 3, where the 2–10 keV luminosity, predicted using the luminosity at  $5.8\mu\text{m}$  (left panel) and  $12.3\mu\text{m}$  (right panel) is plotted against the measured X-ray luminosity; with the term “measured X-ray luminosity” (similarly to Fig. 2), we mean that the source luminosity has been corrected for the effect of absorption, once X-ray spectral analysis is able to provide a reliable estimate for it (filled squares: this work; filled triangles: V06); in all of the remaining cases, no correction has been applied (open squares and triangles). In addition, the filled circle represents source ID 239, which was detected by the *ROSAT* All Sky Survey (RASS; V04). The dotted, short-dashed and long-dashed lines indicate ratios of 1:1, 1:10 and 1:100 between the measured and the predicted X-ray luminosity. The average X-ray luminosities predicted by the two methods are  $\log L_X = 44.02\text{ erg s}^{-1}$  and  $44.48\text{ erg s}^{-1}$  using the F09 and G09 mid-IR vs. X-ray correlation, respectively. For comparison, the average X-ray luminosity assuming the Lutz et al. (2004) relation is  $\log L_X = 44.41\text{ erg s}^{-1}$ , 15 per cent lower than that predicted using G09 correlation.

Overall, it appears evident that in both plots two main source groups are present: the right-most one comprises sources which are more or less consistent with the 1:1 correlation, especially using the  $(\lambda L_\lambda)_{12.3\mu\text{m}}$  as a proxy of the nuclear emission (see below for an extended discussion). X-ray spectral analysis indicates that these

sources are Compton-thin AGN and are the same residing close to the 1:1 correlation in Fig. 2. The left-most group regards sources where the expected 2–10 keV luminosity is a factor  $\approx 10$ –100 higher than the measured X-ray luminosity. All but one of these sources are also among the most extreme objects (i.e., candidate Compton-thick AGN) shown in Fig. 2; the only exception is source ID 30, which seems to be Compton thin from hardness-ratio analysis (see §2.2). However, it is evident from Fig. 3 (left panel) that, for the Compton-thin Type 2 quasars of our sample, using the correlation proposed by F09 provides an offset by a factor  $\approx 3$  with respect to the X-ray measured/intrinsic 1:1 luminosity ratio, while the G09 correlation seems to produce a good match with the luminosity ratio of unity (Fig. 3, right panel), hence with the results obtained from [O III] analysis. Although clearly mid-IR vs. X-ray correlations need to be investigated further on larger samples to achieve a more accurate “calibration”, we note that, at the measured X-ray luminosities sampled by the SDSS Compton-thin Type 2 quasars (i.e., above  $10^{44}\text{ erg s}^{-1}$ ), the dispersion in the F09 correlation seems to be large (see their Fig. 5). By contrast, the correlation presented by G09 has a relative small dispersion (0.36 dex) throughout the entire luminosity range, being smaller for the subsample of 22 well resolved sources (0.23 dex; see §4.1 in G09 for details). Therefore, in the following section, we will report on the results obtained using the information from the [O III] and  $12.3\mu\text{m}$  to predict 2–10 keV luminosities.

Caution is obviously needed when dealing with infrared data, given the likely presence of both AGN (torus) and starburst emission. Although the AGN seems to dominate over the *Spitzer* bands (eight of the 20 sources listed in Table 4 have IRS coverage; see §3.4 of Zakamska et al. 2008 for details), we note that in the derived rest-frame  $5.8\mu\text{m}$  and  $12.3\mu\text{m}$  luminosities there might be some contribution from star formation (see Table 1 of Zakamska et al. 2008). However, we remind that the correlation reported by G09 was obtained using near diffraction-limited mid-IR imaging, where any non-AGN contribution can be observed and kept under control (see also Horst et al. 2009).

Overall, both [O III] and  $12.3\mu\text{m}$  luminosity provide similar indications for what concerns the X-ray emission of SDSS Type 2 quasars, with roughly half of the sampled (i.e., with X-ray coverage) population being possibly Compton-thick (see §4 for further comparison and discussion). Recently, heavy obscuration has also been found in some SDSS Type 2 AGN by Lamastra et al. (2009) using *XMM-Newton* observations; given the low redshifts of their sources, they were able to correct for the extinction within the NLR and provide a tight and robust [O III] vs. hard X-ray correlation.

Finally, we note that *Spitzer* (IRS) follow-up observations of SDSS Type 2 quasars have recently revealed a wealth of mid-infrared properties, with 7/12 sources showing a silicate absorption features at  $10\mu\text{m}$ , suggestive of heavy obscuration toward the source (Zakamska et al. 2008). It is intriguing that the two objects with the most prominent silicate absorption features (SDSS 0056+0032 and SDSS 0815+4304; see Fig. 1 of Zakamska et al. 2008) are candidate Compton-thick quasars accordingly to all methods adopted in this paper to estimate the intrinsic X-ray luminosity, although not all of the SDSS Type 2 quasars which have been classified as Compton-thick according to our analyses were found to show Si absorption (see Fig. 1 of Zakamska et al. 2008). This fact can be explained in clumpy torus models (e.g., Nenkova, Ivezić & Elitzur 2002; Hönig, Beckert & Ohnaka 2006; Nenkova et al. 2008a,b), where the effective infrared optical depth can be decreased by random mis-alignments and holes through the obscuring clouds.

<sup>5</sup> We note that source extraction regions of a few tens arcsec are typically used in *XMM-Newton* observations.



**Table 5.** Classification of Type 2 quasars with  $\log L_{[\text{O III}]} > 9.28 L_{\odot}$ .

ID (1)	Src. Name (2)	$z$ (3)	$L_{X,\text{meas}}/L_{X,[\text{O III}]}$ (4)	$L_{X,\text{meas}}/L_{X,12.3\mu\text{m}}$ (5)	Class. [O III] (6)	Class. 12.3 $\mu\text{m}$ (7)
7	005009.81–003900.6	0.729	0.37	...	thin	...
9	005621.72+003235.8	0.484	1.41E-03	7.41E-04	THICK	THICK
16	012032.21–005502.0	0.601	4.90E-03	...	THICK	...
20	013416.34+001413.6	0.555	1.58E-03	3.39E-03	THICK	THICK
29	014932.53–004803.7	0.566	<4.27E-03	...	THICK	...
30	015716.92–005304.8	0.422	7.08E-03	5.01E-02	interm	thin
34	021047.01–100152.9	0.540	0.16	0.87	thin	thin
83	031950.54–005850.6	0.626	4.37E-03	1.78E-02	THICK	thin
100	073745.88+402146.5	0.613	7.08E-03	...	THICK	...
113	080154.24+441234.0	0.556	0.49	1.3	thin	thin
119	081507.42+430427.2	0.510	<3.89E-03	<4.79E-03	THICK	THICK
130	084234.94+362503.1	0.561	<2.75E-03	<2.88E-02	THICK	interm
153	092152.45+515348.1	0.587	<5.37E-03	...	THICK	...
182	102746.03+003205.0	0.614	3.09E-03	...	THICK	...
186	103951.49+643004.2	0.402	2.09E-03	2.00E-03	THICK	THICK
196	115314.36+032658.6	0.575	0.13	0.47	thin	thin
197	115718.35+600345.6	0.491	<1.70E-03	<1.02E-03	THICK	THICK
204	122656.48+013124.3	0.732	0.42	0.89	thin	thin
205	122845.74+005018.7	0.575	8.13E-02	...	thin	...
207	123215.81+020610.0	0.480	1.82E-03	8.51E-03	THICK	THICK
232	144642.29+011303.0	0.725	9.55E-03	...	THICK	...
244	151711.47+033100.2	0.613	2.95E-03	...	THICK	...
256	164131.73+385840.9	0.596	0.40	1.0	thin	thin
289	235818.87–000919.5	0.402	<6.61E-03	<2.88E-02	THICK	interm
290	235831.16–002226.5	0.628	1.58E-03	3.98E-02	THICK	thin

(1) Source ID (from Table 1 of Z03); (2) SDSS source name; (3) source redshift; (4) ratio of the measured 2–10 keV luminosity and that predicted from the [O III]5007Å luminosity assuming the M94 correlation; (5) ratio of the measured 2–10 keV luminosity and that predicted from the 12.3 $\mu\text{m}$  luminosity (when available; see Table 4) assuming the G09 correlation; (6) tentative source classification on the basis of the measured/predicted (from the [O III]) luminosity ratio. For source #30, although a Compton-thick classification is derived from the luminosity ratio, hardness-ratio analysis (§2.2) suggests Compton-thin obscuration; (7) tentative source classification on the basis of the measured/predicted (from the 12.3 $\mu\text{m}$ ) luminosity ratio; objects are classified as “intermediate” if the upper limit on the luminosity ratio prevents any conclusion.

#### 4 NUMBER DENSITY OF SDSS COMPTON-THICK QUASARS

It is now interesting to compute the space density of candidate Compton-thick Type 2 quasars selected by the SDSS and compare it with that of other samples of Compton-thick AGN candidates and with the predictions by synthesis models of the XRB. First, we considered the complete sub-sample of radio-quiet objects presented in V06 and in this work with  $\log L_{[\text{O III}]} > 9.28 L_{\odot}$  (therefore source SDSS 0812+4018 has been removed because it is radio loud; see §2): six objects fall in the redshift range  $z = 0.3 - 0.5$  [with 5 objects being Compton-thick candidates using the X-ray measured/predicted (from [O III]) luminosity ratio,  $L_{X,\text{meas}}/L_{X,[\text{O III}]}$ ] and 19 objects fall in the redshift range  $z = 0.5 - 0.8$  (with 12 objects being Compton-thick candidates, still according to [O III]); the properties of these sources are summarized in Table 5.

Before entering into the details of the number density computation, we remind the reader that we refer to a Compton-thick quasar when the ratio of the measured to predicted X-ray luminosity is less than 0.01. On the basis of the  $L_{X,\text{meas}}/L_{X,[\text{O III}]}$  ratio, the X-ray emission for 17 of the 25 Type 2 quasars in our sample (68 per cent) appears to be obscured by Compton-thick material. However, since the Type 2 quasar sample is selected on [O III] luminosity, the estimated Compton-thick quasar fraction may be overestimated. We can provide an indication of the

“[O III] bias” by determining the fraction of the Type 2 quasars that are classified as Compton thick based on both the X-ray/[O III] and X-ray/mid-IR ratios. Of the 16 Type 2 quasars with archival *Spitzer* observations and  $\log L_{[\text{O III}]} > 9.28 L_{\odot}$  (see Table 5), 10 have  $L_{X,\text{meas}}/L_{X,[\text{O III}]} < 0.01$ , of which 6 (60 per cent) also have  $L_{X,\text{meas}}/L_{X,\text{mid-IR}} < 0.01$  (where mid-IR is based on 12.3 $\mu\text{m}$ ); however, two objects have X-ray/mid-IR upper limits which are slightly above our Compton-thick quasar definition (“intermediate” in Table 5), suggesting that the fraction of Compton-thick quasars may be 75 per cent (i.e., 6 out of 8 objects).

Overall, our analyses therefore suggest that the unbiased Compton-thick quasar fraction is  $\approx 50$  per cent.<sup>6</sup>

In our calculation below, we will refer to the [O III] indicator to compute the number density of SDSS Compton-thick quasars,

<sup>6</sup> The current study indicates that, for the 14 sources with [O III] and 12.3 $\mu\text{m}$  indicators (16 objects minus two classified as “intermediate” in the mid-IR), [O III] is highly reliable in classifying sources as Compton-thick in at least 75 per cent of the cases (since source #83 has a “borderline” classification as Compton thin according to the 12.3 $\mu\text{m}$  indicator). Applying this “correction factor” to the number of Compton-thick sources with only [O III] as reliable indicator (i.e., no solid mid-IR information) implies at least 7 Compton-thick quasars out of 9 (hence, 13/25 for the sample under investigation).

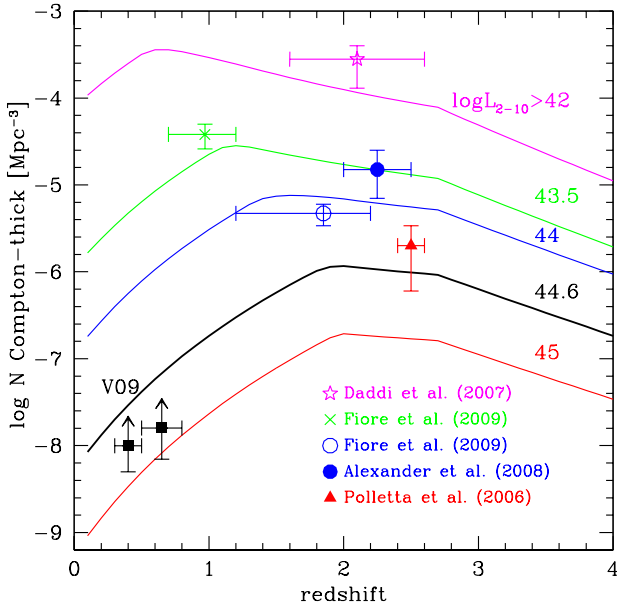


**Figure 4.** Volume density of Compton-thick AGN samples with different intrinsic 2–10 keV luminosities compared with the XRB model predictions (Gilli et al. 2007). Data points refer to this work (filled squares at low redshift with upward-pointing arrows) and literature work (all the other symbols, at  $z \approx 1 - 2.5$ ; reference papers are listed in the bottom part of the figure), and have to be compared with the corresponding color curves.

since it is available for all of the 25 sources under consideration; however, any correction to the [O III] bias would decrease our estimate by  $\approx 25$  per cent at most.

Recently, R08 published an extended list of SDSS Type 2 AGN candidates. They also reported new values for the [O III] line luminosity, which is measured using both a fitting with a Gaussian feature and with a non-parametric method (see Section 2.4 of R08 for a detailed description), besides adopting the most up-to-date spectro-photometric calibration algorithm from the SDSS. Since our project was originally intended to provide an X-ray characterization of all of the sources of the Z03 sample in the quasar locus (i.e., at high X-ray luminosities, predicted accordingly to the [O III] vs. hard X-ray correlation of M94; see Fig. 1), in the following we will keep the original [O III] line luminosity reported by Z03. However, it is interesting to analyze thoroughly what the main differences would be in case of source selection on the basis of the [O III] line luminosity as reported in R08. If we adopt the same selection of  $\log L_{[\text{O III}]} > 9.28 L_{\odot}$  using the R08 source catalog instead of the original catalog of Z03, we obtain a sample comprising 26 sources, 22 in common with the source list reported in Table 5. On the one hand, sources #16, #30 and #244 (two classified as Compton thick on the basis of [O III] only, and one as intermediate/Compton-thin) would not be present anymore for our estimates of the volume density of SDSS Compton-thick quasars. On the other hand, sources #117, #141, #189 and #213 would be included. While source #117 must be removed because of its radio loudness (its exclusion was described at the beginning of this Section), a similar destiny would be reserved to source #189, for the same reason. The other two sources lack any X-ray constrain to date, so they would not be useful for the following analysis. In the light of the limited number of changes implied by the adoption of the R08 catalog (and the way we account for the Compton-thick

AGN predicted using only [O III], as described above), we are confident that the main conclusions of the present work (reported in the following paragraphs) will not change significantly. We also note that, for the sources above the chosen [O III] line luminosity threshold in both catalogs (22 objects), the logarithms of the luminosities derived for [O III] differ, on average, by  $\approx 0.09$ , with no obvious evidence for systematic effects.

In order to get the space density of Type 2 quasars above the chosen luminosity threshold, we integrated the SDSS Type 2 quasars luminosity function published by R08 from  $\log L_{[\text{O III}]} > 9.28 L_{\odot}$  to the maximum luminosity for which they have data, i.e.  $\log L_{[\text{O III}]} = 10.3 L_{\odot}$  and  $\log L_{[\text{O III}]} = 10.0 L_{\odot}$  for objects in the range  $z = 0.3 - 0.5$  and  $z = 0.5 - 0.8$ , respectively. For the objects in the  $z = 0.5 - 0.8$  bin, we considered both curves in Fig. 5 of R08, in which the measured space densities depend on a different correction applied to the Type 2 quasar selection function (see R08 for details). These integrations return a space density of  $1.2 \times 10^{-8} \text{ Mpc}^{-3}$  for Type 2 quasars at  $z = 0.3 - 0.5$  and  $(1.9 - 2.6) \times 10^{-8} \text{ Mpc}^{-3}$  (depending on the correction mentioned above) for Type 2 quasars at  $z = 0.5 - 0.8$ . Since 5 out of 6 objects in our  $z = 0.3 - 0.5$  sample and 12 out of 19 objects in our  $z = 0.5 - 0.8$  sample are Compton-thick candidates, we estimate the space densities of [O III]-selected SDSS Compton-thick quasars to be  $1.2 \times 10^{-8} \times (5/6) = 10^{-8} \text{ Mpc}^{-3}$  and  $(1.9 - 2.6) \times 10^{-8} \times (12/19) = (1.2 - 1.6) \times 10^{-8} \text{ Mpc}^{-3}$ , at  $z = 0.3 - 0.5$  and  $z = 0.5 - 0.8$ , respectively. Based on the observed [O III] vs. intrinsic  $L_{2-10\text{keV}}$  relations published by M94, the above space densities should then refer to Type 2 quasars with  $\log L_X > 44.6 \text{ erg s}^{-1}$ . In Fig. 4 we show the comparison between the space densities derived for our sample and those published for other samples of Compton-thick AGN candidates at different redshifts and luminosities. The densities presented in this work cover a corner in the luminosity vs. redshift plane of Compton-thick AGN so far unexplored. We also show the expected redshift evolution of the space density of Compton-thick AGN with different intrinsic luminosities based on the XRB model of Gilli et al. (2007). Our measurements are about a factor of 2–3 lower than the expectations of the XRB model, in which Type 2 Compton-thick quasars are assumed to be as abundant as unobscured quasars with the same intrinsic luminosity. A number of Compton-thick AGN smaller than expected (by a factor of 2, corresponding to  $\approx 2\sigma$ ) might also be suggested by recent *Integral* (Beckmann et al. 2009) and *Swift* (Tueller et al. 2008) surveys of very local objects, which would point towards a revision of the XRB models (although this issue is still matter of debate, see Malizia et al. 2009). For instance, a lower space density of Compton-thick AGN features the recent model by Treister, Urry & Virani (2009).

A few caveats have nonetheless to be kept in mind: indeed, R08 consider their estimates to be lower limits, since, if the NLR is extinguished, a significant fraction of obscured AGN may escape detection based on narrow optical emission lines (other arguments are discussed in R08). In addition, the intrinsic X-ray luminosity of these Compton-thick Type 2 quasar candidates has been obtained using an observed [O III] vs. intrinsic X-ray luminosity relation derived by M94 for a local sample of Seyferts, which generally cover a lower [O III] luminosity range, and have not been selected on the basis of their [O III] flux or luminosity. As mentioned in §2.3, other relations between [O III] and X-ray luminosities have been published by H05 and P06, but none of them is based on a purely [O III] selected sample, although H05 made an attempt to build a sample of [O III]-bright local Seyferts as a surrogate. For their sample of Seyfert 1 objects, i.e. for those sources in which the intrinsic X-ray

emission can be estimated directly, H05 derived X-ray luminosities on average a factor of 1.5 lower than those derived by M94 at a given [O III] luminosity [ $\log L_X/L_{[\text{OIII}]}=1.59$  vs 1.76]. Therefore, using the relation by H05 we would estimate for our sources intrinsic luminosities of  $\log L_X > 44.4 \text{ erg s}^{-1}$ . In the considered XRB synthesis model, the space density of obscured AGN, and therefore also of Compton-thick AGN, is expected to increase with decreasing intrinsic luminosity. At  $z = 0.3 - 0.8$ , the XRB space density of Compton-thick AGN with  $\log L_X > 44.4 \text{ erg s}^{-1}$  is expected to be about an order of magnitude larger than that measured in this work. On the other hand, when using the relation by P06, which is essentially based on optically selected AGN samples, the [O III] luminosity threshold translates into an X-ray luminosity threshold of  $\log L_X > 44.8 \text{ erg s}^{-1}$ . At these luminosities, the model space density of Compton-thick Type 2 quasars is very close to our measurements. Summarizing, given the uncertainties mentioned above (see also § 2.3), at  $z = 0.3 - 0.8$ , Compton-thick Type 2 quasars selected by the SDSS are compatible with being as abundant as unobscured quasars of similar luminosities (see also Alexander et al. 2008).

## 5 SUMMARY

We have presented the most up-to-date results regarding the properties of Type 2 quasar candidates selected from the SDSS and observed by *Chandra*. In particular, the objects presented in this work consists on two samples, one comprising 12 Type 2 quasars selected in *Chandra* Cycle 8 among the most luminous [O III] emitters, and the other comprising three additional candidates at lower [O III] luminosity retrieved from the *Chandra* archive. The full sample spans the redshift range  $z=0.40-0.73$ . The main results are summarized below:

- Our *Chandra* exploratory observations ( $\approx 10$  ks for each pointing) support previous findings that SDSS Type 2 quasars are X-ray faint: two sources were not detected by *Chandra* and nine of the detected sources have less than 10 counts in the observed 0.5–8 keV band. For only three sources it was possible to perform a low-to-moderate quality spectral analysis, providing evidence for column densities in the range  $N_{\text{H}} \approx 10^{22}-10^{23} \text{ cm}^{-2}$  in the source rest frame.

- The assumption of the [O III] luminosity as a proxy of the nuclear emission, coupled with literature [O III]–hard X-ray correlations (with all the caveats of this approach being extensively discussed in §2.3 and §4), indicates that a significant fraction (about two-third) of the SDSS Type 2 quasars with  $\log L_{[\text{O III}]} > 9.28 L_{\odot}$  presented here and in V06 may be Compton thick (see also Ptak et al. 2006 and Lamastra et al. 2009).

- Further indications of heavy obscuration in a sizable fraction of SDSS Type 2 quasars come from the analysis of archival *Spitzer* observations, which have been used to estimate the intrinsic (i.e., de-absorbed) hard X-ray AGN strength assuming some recent correlations between either the rest-frame  $5.8\mu\text{m}$  or the  $12.3\mu\text{m}$  luminosity and the 2–10 keV luminosity. Using the combined [O III], mid-IR and X-ray information (by means of luminosity ratios; see Table 5) it is possible to distinguish the Compton-thick from the Compton-thin Type 2 quasar population. Overall, we find that  $\approx 50$  per cent of SDSS Type 2 quasars with  $\log L_{[\text{O III}]} > 9.28 L_{\odot}$  appear to be obscured by Compton-thick material based on both the  $L_{X,\text{meas}}/L_{X,\text{mid-IR}}$  (where mid-IR corresponds to rest-frame  $12.3\mu\text{m}$ ) and  $L_{X,\text{meas}}/L_{X,[\text{OIII}]}$  ratios. Moderate-quality X-ray spectra showing a strong iron  $\text{K}\alpha$  emission line over a flat continuum

would provide a further, clean indication of Compton-thick absorption. However, given the low X-ray fluxes of these sources, such spectral approach, extended to sizable samples, probably demands next-generation of sensitive X-ray detectors.

- By integrating the SDSS Type 2 quasar luminosity function of R08 above  $\log L_{[\text{OIII}]} > 9.28 L_{\odot}$  (corresponding to  $\log L_X > 44.6 \text{ erg s}^{-1}$  under the assumption of the M94 relation; see Fig. 1), we obtain an estimate of the space density of Type 2 quasars above this luminosity threshold of  $\approx 10^{-8} \text{ Mpc}^{-3}$  and  $\approx (1.2 - 1.6) \times 10^{-8} \text{ Mpc}^{-3}$  at  $z = 0.3 - 0.5$  and  $z = 0.5 - 0.8$ , respectively. At face value, these space densities are a factor 2–3 lower than the expectations of the XRB model by Gilli et al. (2007) and would suggest that Compton-thick Type 2 quasars are less abundant than unobscured quasars (Treister et al. 2009). However, given the uncertainties in the SDSS Type 2 quasar luminosity function (mainly related to possible extinction within the NLR) and in the assumption of the [O III]–hard X-ray correlation (see §4), we can conclude that the estimated space density of SDSS Compton-thick Type 2 quasars at  $z = 0.3 - 0.8$  is likely a lower limit. In other words, in this still poorly explored redshift range (recent results on space densities of heavily obscured quasars are mostly at  $z \approx 1 - 2.5$ ), Compton-thick Type 2 quasars are consistent with being as abundant as unobscured quasars of similar intrinsic luminosities.

## ACKNOWLEDGMENTS

CV and RG thank for partial support the Italian Space Agency (contracts ASI-INAF I/023/05/0 and ASI I/088/06/0) and PRIN–MIUR (grant 2006-02-5203). DMA acknowledges support by the Royal Society and the Leverhulme Trust. The authors thank S. Bianchi, A. Comastri, R. Della Ceca, P. Gandhi, A. Lamastra, G. Matt, F. Panessa, G. C. Perola, M. Polletta and G. Zamorani for useful suggestions, and M. Mignoli for help with SDSS Type 2 quasar spectra, and the anonymous referee for his/her careful reading of the manuscript and useful comments.

## REFERENCES

- Alexander D.M., Chartas G., Bauer F.E., Brandt W.N., Simpson C., Vignali C., 2005, MNRAS, 357, L16  
 Alexander D.M. et al., 2008, ApJ, 687, 835  
 Antonucci R., 1993, ARA&A, 31, 473  
 Arnaud K.A., 1996, in Jacoby G., Barnes J., eds, ASP Conf. Ser. Vol. 101, Astronomical Data Analysis Software and Systems V. Astron. Soc. Pac., San Francisco, p. 17  
 Avni Y., 1976, ApJ, 210, 642  
 Bassani L., Dadina M., Maiolino R., Salvati M., Risaliti G., della Ceca R., Matt G., Zamorani G., 1999, ApJS, 121, 473  
 Becker R.H., White R.L., Helfand D.J., 1995, ApJ, 450, 559  
 Beckmann V. et al., 2009, A&A, 505, 417  
 Brusa M. et al., 2010, A&A, submitted  
 Cash W. 1979, ApJ, 228, 939  
 Comastri A., 2004, in “Supermassive Black Holes in the Distant Universe”, ed. A.J. Barger, Kluwer Academic Press, Vol. 308, p. 245  
 Condon J.J., Cotton W.D., Greisen E.W., Yin Q.F., Perley R.A., Taylor G.B., Broderick J.J., 1998, AJ, 115, 1693  
 Daddi E. et al., 2007, ApJ, 670, 173  
 Della Ceca R. et al., 2008, A&A, 487, 119  
 Dey A. et al. 2008, ApJ, 677, 943  
 Dickey J.M., Lockman F.J., 1990, ARA&A, 28, 215  
 Donley J.L. et al., 2008, ApJ, 687, 111  
 Fiore F. et al., 2003, A&A, 409, 79

- Fiore F. et al., 2008, *ApJ*, 672, 94  
 Fiore F. et al., 2009, *ApJ*, 693, 447 (F09)  
 Freeman P.E., Kashyap V., Rosner R., Lamb D.Q., 2002, *ApJS*, 138, 185  
 Gandhi P., Crawford C.S., Fabian A.C., Johnstone R.M., 2004, *MNRAS*, 348, 529  
 Gandhi P., Fabian A.C., Crawford C.S., 2006, *MNRAS*, 369, 1566  
 Gandhi P., Horst H., Smette A., Hönig S., Comastri A., Gilli R., Vignali C., Duschl W., 2009, *A&A*, 502, 457 (G09)  
 Garmire G.P., Bautz M.W., Ford P.G., Nousek J.A., Ricker G.R., 2003, *Proc. SPIE*, 4851, 28  
 Gehrels N., 1986, *ApJ*, 303, 336  
 Gilli R., Comastri A., Hasinger G., 2007, *A&A*, 463, 79  
 Heckman T.M., Ptak A., Hornschemeier A., Kauffmann G., 2005, *ApJ*, 634, 161 (H05)  
 Higdon J.L. et al., 2005, *ApJ*, 626, 58  
 Higdon J.L., Higdon S.J.U., Willner S.P., Brown M.J., Stern D., Le Floch E., Eisenhardt P., 2008, *ApJ*, 688, 885  
 Hönig S.F., Beckert T., Ohnaka K., Weigelt G., 2006, *A&A*, 452, 459  
 Horst H., Smette A., Gandhi P., Duschl W.J., 2006, *A&A*, 457, L17  
 Horst H., Gandhi P., Smette A., Duschl W.J., 2008, *A&A*, 479, 389  
 Horst H., Duschl W.J., Gandhi P., Smette A., 2009, *A&A*, 495, 137  
 Houck J.R. et al., 2005, *ApJ*, 622, L105  
 Kellermann K.L., Sramek R., Schmidt M., Shaffer D.B., Green R.F., 1989, *AJ*, 98, 1195  
 Kraft R.P., Burrows D.N., Nousek J.A., 1991, *ApJ*, 374, 344  
 Krumpe M. et al., 2008, *A&A*, 483, 415  
 LaMassa S.M., Heckman T.M., Ptak A., Hornschemeier A., Martins L., Sonnentrucker P., Tremonti C., 2009, *ApJ*, 705, 568  
 Lamastra A., Bianchi S., Matt G., Perola G.C., Barcons X., Carrera F.J., 2009, *A&A*, 504, 73  
 Lanzuisi G., Piconcelli E., Fiore F., Feruglio C., Vignali C., Salvato M., Gruppioni C., 2009, *A&A*, 498, 67  
 Liu X., Zakamska N.L., Greene J.E., Strauss M.A., Krolik J.H., Heckman T.M., 2009, *ApJ*, 702, 1098  
 Lutz D., Maiolino R., Spoon H.W.W., Moorwood, A.F.M., 2004, *A&A*, 418, 465  
 Mainieri V. et al., 2002, *A&A*, 393, 425  
 Mainieri V. et al., 2007, *ApJS*, 172, 368  
 Maiolino R., Salvati M., Bassani L., Dadina M., della Ceca R., Matt G., Risaliti G., Zamorani G., 1998, *A&A*, 338, 781  
 Malizia A., Stephen J.B., Bassani L., Bird A.J., Panessa F., Ubertini P., 2009, *MNRAS*, 399, 944  
 Martínez-Sansigre A., Rawlings S., Lacy M., Fadda D., Marleau F.R., Simpson C., Willott C.J., Jarvis M.J., 2005, *Nature*, 436, 666  
 Martínez-Sansigre A. et al., 2007, *MNRAS*, 379, L6  
 Martínez-Sansigre A., Lacy M., Sajina A., Rawlings S., 2008, *ApJ*, 674, 676  
 Mateos S., Barcons X., Carrera F.J., Ceballos M.T., Hasinger G., Lehmann I., Fabian A.C., Streblyanska A., 2005, *A&A*, 444, 79  
 Matt G., Fabian A.C., Guainazzi M., Iwasawa K., Bassani L., Malaguti G., 2000, *MNRAS*, 318, 173  
 Mulchaey J.S. et al., 1994, *ApJ*, 436, 586 (M94)  
 Nenkova M., Ivezić Ž., Elitzur M., 2002, *ApJ*, 570, L9  
 Nenkova M., Sirocky M. M., Ivezić Ž., Elitzur M., 2008a, *ApJ*, 685, 147  
 Nenkova M., Sirocky M. M., Nikutta R., Ivezić Ž., Elitzur M., 2008b, *ApJ*, 685, 160  
 Norman C. et al., 2002, *ApJ*, 571, 218  
 Nousek J.A., Shue D.R., 1989, *ApJ*, 342, 1207  
 Page K.L., Reeves J.N., O'Brien P.T., Turner M.J.L., 2005, *MNRAS*, 364, 195  
 Panessa F., Bassani L., Cappi M., Dadina M., Barcons X., Carrera F.J., Ho L.C., Iwasawa K., 2006, *A&A*, 455, 173 (P06)  
 Piconcelli E., Jimenez-Bailón E., Guainazzi M., Schartel N., Rodríguez-Pascual P.M., Santos-Lleó M., 2005, *A&A*, 432, 15  
 Polletta M. et al., 2006, *ApJ*, 642, 673  
 Polletta M. et al., 2008, *A&A*, 492, 81  
 Ptak A., Zakamska N.L., Strauss M.A., Krolik J.H., Heckman T.M., Schneider D.P., Brinkmann J., 2006, *ApJ*, 637, 147  
 Reyes R. et al., 2008, *AJ*, 136, 2373 (R08)  
 Severgnini P. et al., 2006, *A&A*, 451, 859  
 Spergel D.N. et al., 2003, *ApJS*, 148, 175  
 Treister E., Urry C.M., Virani S., 2009, *ApJ*, 696, 110  
 Tueller J., Mushotzky R.F., Barthelmy S., Cannizzo J.K., Gehrels N., Markwardt C.B., Skinner G.K., Winter L.M., 2008, *ApJ*, 681, 113  
 Vignali C., Brandt W.N., Fan X., Gunn J.E., Kaspi S., Schneider D.P., Strauss M.A., 2001, *AJ*, 122, 2143  
 Vignali C., Alexander D.M., Comastri A., 2004a, *MNRAS*, 354, 720 (V04)  
 Vignali C., Alexander D.M., Comastri A., 2004b, proceedings of the 6<sup>th</sup> Italian National Meeting on AGN electronic edition at <http://www.arcetri.astro.it/~agn6/> (astro-ph/0409699)  
 Vignali C., Alexander D.M., Comastri A., 2006, *MNRAS*, 373, 321 (V06)  
 Villar-Martín M., Humphrey A., Martínez-Sansigre A., Pérez-Torres M., Binette L., Zhang X.G., 2008, *MNRAS*, 390, 218  
 Weedman D.W., Le Floch E., Higdon S.J.U., Higdon J.L., Houck J.R., 2006a, *ApJ*, 638, 613  
 Weedman D.W. et al., 2006b, *ApJ*, 651, 101  
 Weedman D. et al., 2006c, *ApJ*, 653, 101  
 York D.G. et al., 2000, *ApJ*, 120, 1579  
 Zakamska N.L. et al., 2003, *ApJ*, 126, 2125 (Z03)  
 Zakamska N.L., Strauss M.A., Heckman T.M., Ivezić Ž., Krolik J.H., 2004, *AJ*, 128, 1002  
 Zakamska N.L. et al., 2005, *AJ*, 129, 1212  
 Zakamska N.L. et al., 2006, *AJ*, 132, 1496  
 Zakamska N.L., Gómez L., Strauss M.A., Krolik J.H., 2008, *AJ*, 136, 1607